TRANSFORMATION ELASTOGRAPHY: CONVERTING ANISOTROPY TO ISOTROPY

Martina Guidetti, Dieter Klatt, Thomas J. Royston

Richard and Loan Hill Department of Bioengineering, University of Illinois at Chicago

ABSTRACT

Elastography refers to mapping mechanical properties in a material based on measuring wave motion in it using noninvasive optical, acoustic or magnetic resonance imaging methods. For example, increased stiffness will increase wavelength. Stiffness and viscosity can depend on both location and direction. A material with aligned fibers or layers may have different stiffness and viscosity values along the fibers or layers versus across them. Converting wave measurements into a mechanical property map or image is known as reconstruction. To make the reconstruction problem analytically tractable, isotropy and homogeneity are often assumed, and the effects of finite boundaries are ignored. But, infinite isotropic homogeneity is not the situation in most cases of interest, when there are pathological conditions, material faults or hidden anomalies that are not uniformly distributed in fibrous or layered structures of finite dimension. Introduction of anisotropy, inhomogeneity and finite boundaries complicates the analysis forcing the abandonment of analytically-driven strategies, in favor of numerical approximations that may be computationally expensive and yield less physical insight. A new strategy, Transformation Elastography (TE), is proposed that involves spatial distortion in order to make an anisotropic problem become isotropic. The fundamental underpinnings of TE have been proven in forward simulation problems. In the present paper a TE approach to inversion and reconstruction is introduced and validated based on numerical finite element simulations.

Index Terms— Elastography imaging; Viscoelasticity imaging; Inverse methods

1. INTRODUCTION

Application of dynamic elastography to tissues with aligned fibrous structure resulting in local transverse isotropic mechanical properties, such as can be found in striated skeletal and cardiac muscle, as well as brain white matter, may benefit from analysis that takes into consideration anisotropy of the tissue. Recognizing this, many groups have pioneered research in this direction over the past few decades, using ultrasound (US)-based elastography [1-2], as well as magnetic resonance (MR)-based elastography [3-4]. Many of these studies have tried to tackle the associated inversion problem. Multiple configurations or a multi-directional shear wave excitation source may be needed in order to generate

and measure shear wave motion that will be affected by its displacement polarization direction and propagation direction in an anisotropic material.

A theoretical approach was recently introduced for the "forward" problem of predicting the slow [5-6] and fast [7] shear wave pattern created by radially converging [5] or diverging [6] shear wave fields in a cylindrical geometry. This approach, referred to as Transformation Elastography (TE), is based on the idea of spatial distortion in order to make the anisotropic problem become isotropic. In the present study using numerical finite element simulations, the approach is inverted, with the aim of eventually making it translatable to analysis of clinical (experimental) data.

2. TRANSVERSE ISOTROPY

Building upon Tweten et al. [8-9], we start with a linear elastic incompressible, transversely isotropic (ITI) material as our model for biological tissue with aligned fibrous structure subjected to deformation that is sufficiently small in amplitude to justify the assumption of linearity. A linear elastic ITI material may be fully described using three parameters which can be a combination of two tensile moduli, E_{\perp} and E_{\parallel} , and two shear moduli, μ_{\perp} and μ_{\parallel} , where the subscripts denote whether the principle direction is perpendicular or parallel to the fiber direction. In other words, E_{\perp} and μ_{\perp} are in the direction perpendicular to the fibers (parallel to the plane of isotropy), and E_{\parallel} and μ_{\parallel} are in the direction parallel to the fibers (parallel to the axis of isotropy). We define shear anisotropy $\phi = \mu_{\parallel}/\mu_{\perp} - 1$ and tensile anisotropy $\zeta = E_{\parallel}/E_{\perp} - 1$. Note also that [10] $E_{\parallel} =$ $\mu_1(4\zeta + 3)$; thus, there are only three independent parameters.

Consider a shear wave traveling in an ITI material with an arbitrary propagation direction that is an angle θ from the fiber direction. The displacement of this shear wave can be polarized into independent slow and fast shear wave components. The polarization direction of the slow shear wave occurs in the direction perpendicular to both the fiber direction and the propagation direction. If the fibers are in the y direction and propagation is in the x-y plane, the polarization will be in the z direction for the slow shear wave. Because the slow shear wave does not stretch the fibers, the speed of the slow shear wave c_s only depends on the shear anisotropy and is given by:

$$c_s^2 = \frac{1}{\rho} (1 + \phi \cos^2[\theta]) \tag{1}$$

The corresponding slow shear wavelength λ_s at frequency f in Hertz is given by $\lambda_s = c_s/f$ and the corresponding wavenumber is $k_s = 2\pi/\lambda_s$. The ratio of the slow shear wavelength parallel to the fibers $\lambda_{s\parallel}$ to the slow shear wavelength perpendicular to the fibers $\lambda_{s\perp}$ is $\lambda_{s\parallel}/\lambda_{s\perp} = \sqrt{1+\phi}$.

On the other hand, for the case of the fast shear wave whose polarization direction is perpendicular to the propagation direction but also perpendicular to the slow shear wave polarization direction, and thus not perpendicular to the fiber direction, we have the speed of the fast shear wave c_f given by:

$$c_f^2 = \frac{\mu_\perp}{\rho} (1 + \phi \cos^2[2\theta] + \zeta \sin^2[2\theta]).$$
 (2)

The corresponding fast shear wavelength λ_f at frequency f in Hertz is given by $\lambda_f = c_f/f$. Note that if $\zeta = \phi$ then $c_f = \sqrt{\frac{\mu_\perp}{\rho}(1+\phi)}$ or in other words $\lambda_f = \lambda_{s\parallel}$ regardless of θ . If $\zeta \neq \phi$ the relationship is more complex.

With respect to propagation of shear waves over a broad frequency range, soft biological tissue is not linear elastic, but rather linear *viscoelastic*, experiencing rate-dependent energy loss (dissipated as heat) as the wave propagates through the material. Linear viscoelasticity can be accounted for in the above formulation by defining $\mu_{\perp} = \mu_{\perp R} + j\mu_{\perp I}$ and $\mu_{\parallel} = \mu_{\parallel R} + j\mu_{\parallel I}$ where $j = \sqrt{-1}$ and the real parts of μ_{\perp} and μ_{\parallel} denote the shear storage moduli and the imaginary parts denote the shear loss moduli. Both shear storage and loss moduli may be a function of frequency f, possibly governed by a rheological model that establishes their dependence on frequency. With the introduction of complex values for the shear modulus, the corresponding expression for the slow shear wavelengths perpendicular and parallel to the fibers become [11]:

$$\lambda_{\perp} = \frac{1}{f} \sqrt{\frac{2}{\rho} \frac{\mu_{\perp R}^2 + \mu_{\perp I}^2}{\mu_{\perp R} + \sqrt{\mu_{\perp R}^2 + \mu_{\perp I}^2}}}, \lambda_{\parallel} = \frac{1}{f} \sqrt{\frac{2}{\rho} \frac{\mu_{\parallel R}^2 + \mu_{\parallel I}^2}{\mu_{\parallel R} + \sqrt{\mu_{\parallel R}^2 + \mu_{\parallel I}^2}}}. \quad (3-4)$$

3. INVERSION & RECONSTRUCTION STRATEGY

The following approach to inversion and reconstruction for the two-dimensional (2D) problem is proposed:

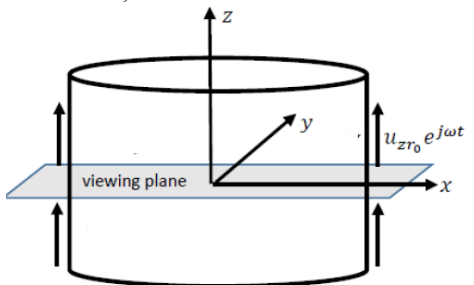
- 1) Acquire the wave field image (and process as needed: filtering, masking near boundaries, etc.) [12];
- Take the image into k-space (2D FFT) and identify dominant wavenumbers;
- 3) Distort the geometry by the wavenumber ratio;
- 4) Proceed with reconstruction assuming isotropy;
- Use the wavenumber ratio to estimate orthotropic properties (the orthotropic ratio).

4. RESULTS: APPLICATION TO 2D PROBLEM

The case study configuration (Fig. 1) is based on an experimental setup used by our group and others to conduct

MRE on biological tissue and phantom material specimens, utilizing geometrically focused (radially converging) shear wave excitation [13-14]. Geometry and material property values, which are typical of soft biological tissue and tissue phantoms are provided in Table I.

A numerical FE study using harmonic analysis (steady state response equivalent to particular solution in the frequency domain) was conducted using COMSOL Multiphysics Version 5.3 (COMSOL, Burlington, MA) software. The automatically meshed model contained 46 724 vertices, 267 162 quadratic tetrahedral elements (0.004 to 0.4 mm in size), 9 152 triangular elements, 328 edge elements and 8 vertex elements. The minimum and average element quality were 0.176 and 0.662, respectively. The element volume ratio was 0.0565 and the mesh volume was 1004 mm³. (Mesh resolution was decided upon when further increases had a negligible effect on the solution.) Typical computation times for the single frequency harmonic analysis were about 30 minutes using a 64-bit operating system, x64 based processor, Intel® Xeon® CPU E5-2609 0 with a clock speed of 2.40 GHz, and 256 GB RAM.



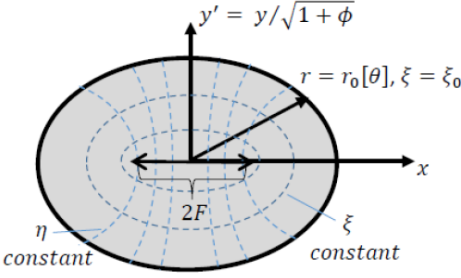
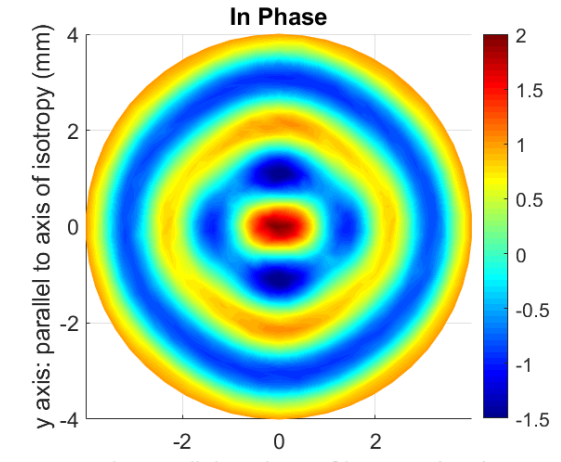


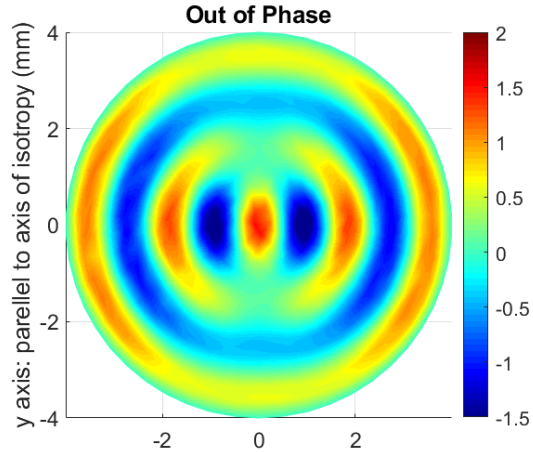
Figure 1. Transversely isotropic cylindrical sample with x-z plane of isotropy (fibers in y direction) subjected to a nonhomogeneous boundary condition: harmonic displacement in the z direction of amplitude u_{zr_0} at frequency $f = \omega/2\pi$ on its curved boundary at $r = r_0$: (a) a 3-dimensional rendering with the x, y "viewing plane" indicated, which is the plane used for Figures 2; (b) viewed in x, y' plane after transformation to an elliptic coordinate system $\{\xi, \eta\}$ with isotropic material properties.

In Fig. 2 we see a comparison of the FE solution for z polarization on an axial slice (x-y plane) with the displacement excitation for the material parameter values in Table 1. Specifically, in Fig. 2a and 2b we see the in and out of phase (with respect to the excitation) responses, respectively.

Parameter	Nomenclature	Value(s)
Cylinder outer radius	r_0	4 mm
Shear storage modulus in	$\mu_{\perp R}$	2.77 kPa
plane of isotropy		
Ratio of shear loss to	$n = \frac{\mu_{\perp I}}{\mu_{\parallel I}} = \frac{\mu_{\parallel I}}{\mu_{\parallel I}}$	0.15
storage moduli	$\eta = \frac{1}{\mu_{\perp R}} = \frac{1}{\mu_{\parallel R}}$	
Shear anisotropy	ϕ	0.3
Tensile anisotropy	ζ	0
Density	ho	$1000 \frac{\text{kg}}{\text{m}^3}$
Frequency	f	1 kHz



x axis: parallel to plane of isotropy (mm)



x axis: parallel to plane of isotropy (mm)

Figure 2. Normalized z direction displacement (u_{zr}/u_{zr_0}) on the x-y plane for z-polarized slow shear waves (a: in phase, b: out of phase).

In Fig. 3, the k-space representation of Figure 2 is shown, acquired via a double Fourier transform and placing the origin at the center via the fftshift command in Matlab. In Fig. 4 estimates of shear storage and loss moduli are shown based on a 2D direct inversion (DI) algorithm. Some discrepancies appear around the cylindrical border due to boundary discontinuities affecting the spatial derivatives used in the DI algorithm. While DI was applied to the distorted geometry, results are plotted for the undistorted geometry.

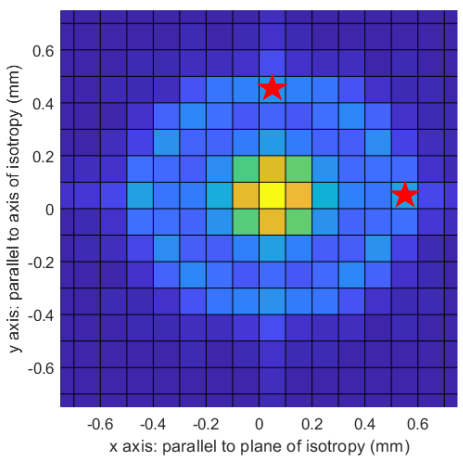
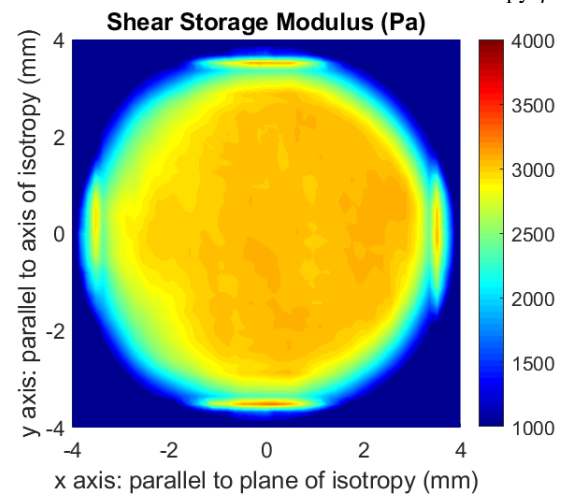


Figure 3. Double Fourier transform of Figure 2 to obtain k-space image. Dominant wavenumbers in k_x and k_y directions indicated with \star . Their ratio is used to estimate the shear anisotropy ϕ .



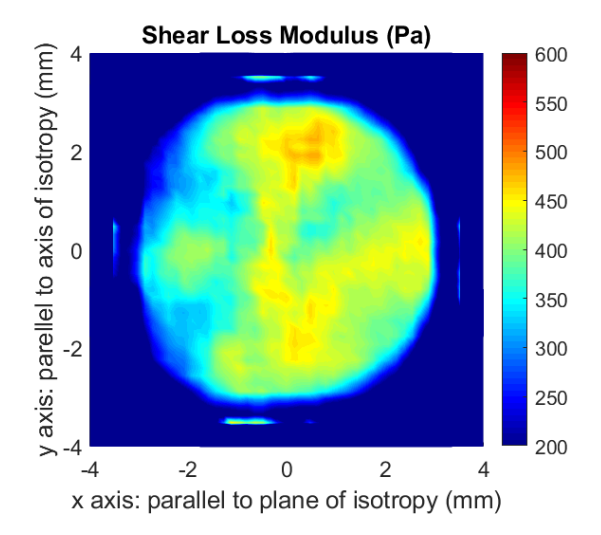


Figure 4. Shear storage and loss moduli estimated using 2D direction inversion on spatially distorted geometry. Undistorted geometry used to plot results.

In Table 2, estimates of the shear storage and loss moduli using Transformation Elastography are shown based on Fig. 4, averaging the values within a 3 mm radius circle centered at the origin to obtain μ_{\perp} , and then multiplying the values by $1+\phi$ to obtain μ_{\parallel} . As a comparison, values are also shown based on assuming isotropy and applying direct inversion to the undistorted geometry with all other aspects of the reconstruction approach the same as in the TE case. Percent error is based on the comparison to the actual values. For the isotropic assumption, two error values are shown reflecting the percent differences with respect to μ_{\perp} and μ_{\parallel} , respectively.

Table 2. Comparison of Material Parameter Estimates

Parameter	Actual Value	Isotropic Assumption (% Error)	Transformation Elastography (% Error)
$\mu_{\perp R}$ (Pa)	2 770	2250 154/249/ 6.09/	3 000 ± 74 (8.3%)
$\mu_{\parallel R}$ (Pa)	3 600	3350 ± 154 (21%, 6.9%)	3 750 ± 93 (4.2%)
$\mu_{\perp I}$ (Pa)	415	472 ± 84.7 (14%, 13%)	399 ± 40 (3.9%)
$\mu_{\parallel I}$ (Pa)	540	472 ± 64.7 (14%, 13%)	499 ± 50 (7.6%)

5. DISCUSSION AND CONCLUSION

A new strategy, Transformation Elastography (TE), is proposed that involves spatial distortion in order to make an anisotropic problem become isotropic. The fundamental underpinnings of TE have been proven in forward simulation problems. In the present paper a TE approach to inversion and reconstruction has been introduced and validated based on numerical finite element (FE) simulations. The FE study results, summarized in Table 2, show that the TE approach provides a more accurate estimate of anisotropic shear storage and loss moduli, as compared to an isotropic assumption, and with minimal additional effort (simply distorting geometry based on a k-space-based estimate of the anisotropic ratio ϕ .

While showing promise, future studies are needed to assess the new strategy in the case of more complex geometries and mechanical wave patterns, including extension to heterogeneous and three-dimensional problems, with experimental noise levels typically found in elastography measurements.

6. ACKNOWLEDGMENTS

NSF #1852691 and NIH #AR071162 funding acknowledged.

7. REFERENCES

[1] S. Chatelin, M. Bernal, T. Deffieux, C. Papadacci, P. Flaud, A. Nahas, C. Boccara, J.-L. Gennisson, M. Tanter, and M. Pernot, "Anisotropic polyvinyl alcohol hydrogel phantom for shear wave elastography in fibrous biological soft tissue: a multimodality characterization," *Phys. Med. Biol.*, vol. 59, pp. 6923–6940, 2014.

- [2] M. Wang, B. Byram, M. Palmeri, N. Rouze, and K. Nightingale, "Imaging transverse isotropic properties of muscle by monitoring acoustic radiation force induced shear waves using a 2-D matrix ultrasound array," *IEEE Trans. Med. Imaging*, vol. 32, pp. 1671-1684, 2013.
- [3] A.J. Romano, P.B. Abraham, P.J. Rossman, J.A. Bucaro, and R.L. Ehman, "Determination and analysis of guided wave propagation using magnetic resonance elastography," *Magn. Reson. Med.*, vol. 54, pp. 893–900, 2005.
- [4] D. Klatt, S. Papazoglou, J. Braun, and I. Sack, "Viscoelasticity-based MR elastography of skeletal muscle," *Phys. Med. Biol.*, vol. 55, pp. 6445–6459, 2010.
- [5] M. Guidetti and T.J. Royston, "Analytical solution for converging elliptic shear wave in a bounded transverse isotropic viscoelastic material with nonhomogeneous outer boundary," *J. Acous. Soc. Am.* vol. 144, pp. 2312–2323, 2018.
- [6] M. Guidetti and T.J. Royston, "Analytical solution for diverging elliptic shear wave in bounded and unbounded transverse isotropic viscoelastic material with nonhomogeneous inner boundary," *J. Acous. Soc. Am.*, vol. 145, pp. EL59–65, 2019.
- [7] M. Guidetti, D. Caratelli, and T.J. Royston, "Converging superelliptic torsional shear waves in a bounded transverse isotropic viscoelastic material with nonhomogeneous outer boundary," *J. Acous. Soc. Am.*, Accepted, 2019.
- [8] D.J. Tweten, R.J. Okamoto, J.L. Schmidt, J.R. Garbow, and P.V. Bayly, "Estimation of material parameters from slow and fast shear waves in an incompressible, transversely isotropic material," *J. Biomech.*, vol. 48, pp. 4002-4009, 2015.
- [9] D.J. Tweten, R.J. Okamoto, P.V. Bayly, "Requirements for Accurate Estimation of Anisotropic Material Parameters by Magnetic Resonance Elastography: A Computational Study," *Magn. Reson. Med.*, vol. 78, pp. 2360–2372, 2017.
- [10] J.L. Schmidt, D.J. Tweten, A.N. Benegal, C.H. Walker, T.E. Portnoi, R.J. Okamoto, J.R. Garbow, and P.V. Bayly, "Magnetic resonance elastography of slow and fast shear waves illuminates differences in shear and tensile moduli in anisotropic tissue," *J. Biomech.*, vol. 49, pp. 1042 1049, 2016.
- [11] S.F. Othman, H. Xu, T.J. Royston, R.L. Magin, "Microscopic Magnetic Resonance Elastography (μ MRE)," *Magn. Reson. Med.*, vol. 54, pp. 605 615, 2005.
- [12] S. Hirsch, J. Braun, I. Sack. *Magnetic Resonance Elastography*. Wiley-VCH, Weinheim, Germany, 2017.
- [13] T.K. Yasar, T.J. Royston, and R.L. Magin, "Wideband MR elastography for viscoelasticity model identification," *Mag. Res. Med.*, vol. 70, pp. 479 489, 2013.
- [14] J. Braun, H. Tzschatzsch, C. Korting, A.A. de Schellenberger, M. Jenderka, T. Driessle, M. Ledwig, and I. Sack, "A compact 0.5 T MR elastography device and its application for studying viscoelasticity changes in biological tissues during progressive formalin fixation," *Magn. Reson. Med.*, vol. 79, pp. 470–478, 2018.